Fall 11-20-2023

Investigating the Diffusion of Solid Yttria Into Solid Zirconia for the Formation of Yttria Stabilized Zirconia

Logan Thomas Ockershausen
logan.ockershausen@student.shu.edu

Investigating the Diffusion of Solid Yttria Into Solid Zirconia for the Formation of Yttria Stabilized Zirconia

By
Logan Thomas Ockershausen

Dissertation Committee
Stephen P. Kelty, Ph.D., Mentor
Mehmet A. Sahiner, Ph.D.
Wyatt R. Murphy, Ph.D.

Submitted to the faculty of the Department of Chemistry and Biochemistry in the School of Arts and Sciences as partial fulfillment of the requirements for the Degree of Masters of Science.

Seton Hall University
400 South Orange Avenue
South Orange, New Jersey 07079

December 2023

We certify that we have read this dissertation and that in our opinion it is adequate in scientific scope and quality as a dissertation for the degree of Masters of Science.

APPROVED

Stephen P. Kelty, Ph.D. Date

Research Mentor, Member of Dissertation Committee, Chair

Department of Chemistry and Biochemistry, Seton Hall University

---

Mehmet A. Sahiner, Ph.D Date

Member of Dissertation Committee, Chair

Department of Physics, Seton Hall University

Wyatt. R. Murphy, Ph.D. Date

Member of Dissertation Committee

Department of Chemistry and Biochemistry, Seton Hall University

Acknowledgements

First and foremost, I would like to thank Dr. Stephen P. Kelty for his mentorship. At the end of my freshman year at Seton Hall, I approached him in his office and explained my interest in computational chemistry. Since then, he has taken me under his wings and showed me the glory of the field. Even when he is being pulled in many different directions as the Department Chair, he still finds time to assist me with whatever I need. I thank you from the bottom of my heart, and I hope that all your wisdom will assist me in my future endeavors.

Secondly, I would like to thank the Kelty research group. Specifically, I would like to thank Tom Melfi and Rory Vander Valk. Tom, your previous work has allowed for my work to continue blossoming and become the very paper you are reading. Rory, whether it was as a TA when I was an undergraduate or as a fellow researcher, you have always been willing and eager to help me with any issues or questions that come up and I thank you for that.

I would also like to thank my friends, especially my fellow graduate students Dani Norguera-Urbina, Isaiah Torres, Jonathan Pinnock, and Josh Korn-Heilner. You have all made my time as a graduate student here at Seton Hall a great experience and one I will always treasure. You have all been a big help from spending time trying to understand topics that are being discussed in class to venting out about some of the students that we teach. I sincerely thank you all.

Last, I would like to give my biggest thanks to my family. Mom, you are the one who helped inspire me to pursue my Master's degree in the first place. You have also worked tirelessly for the entirety of my life so that we could all be happy and healthy. There are no words I have to describe how thankful I am to you. Missy, despite all our bantering and arguing (as all siblings do), I would like to thank you for your support. You have been able to cheer me up when I am

down, and you bring a ray of light into my life that is unquenchable. Thank you both for your endless support and I hope I made you both proud.

Table of Contents

List of Tables

List of Figures

Abstract

A molecular dynamics simulation of yttria-stabilized zirconia (YSZ) is reported in order to analyze the diffusion of the oxygen atoms from the yttria into the zirconia from an initial structure containing a layer of yttria on zirconia. The simulation was performed starting from a pure zirconia slab which was amorphized at the surface followed by placing a slab of yttria on top and a vacuum layer above that. The yttria/zirconia system was simulated at increasing temperatures to 1500K under canonical (NVT) constraints for 6.98 ns until the yttrium atom diffusion was found to occur. The final run was analyzed for oxygen diffusion rates in the region of the system containing 1-10% Y. The oxygen diffusion coefficient was found to be $D=1.35\times10^{-10}$ m^2/s which compares favorably with literature values for bulk oxygen diffusion in YSZ.

Introduction

a) Properties of ZrO_2

Zirconium dioxide (ZrO_2) exists in several crystal phases depending on the temperature. This includes a high symmetry cubic phase, a low symmetry tetragonal phase, and a monoclinic phase. These are depicted in Figure 1.

a) b) c)

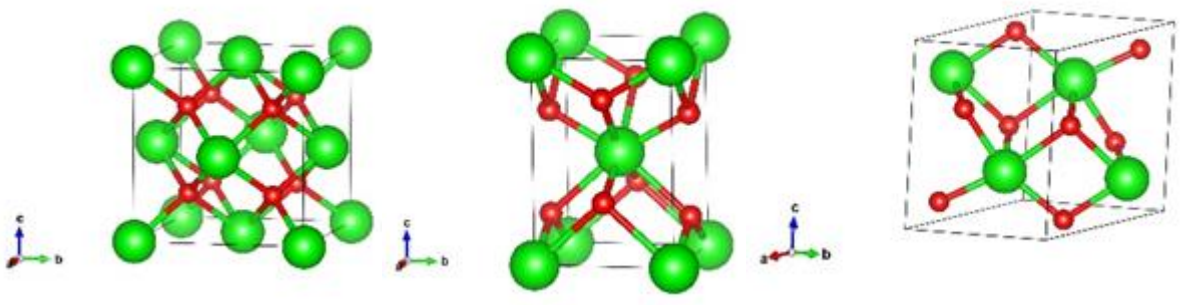

Figure 1. a) cubic, b) tetragonal, and c) monoclinic ZrO_2.

Zirconia has a large number of technical applications due to its low thermal conductivity and its ability for oxygen to migrate within the crystal. The latter property makes it useful for solid oxide electrolytes in fuel cells (SOFC) which require oxygen anions to flow from the cathode to the anode through a solid oxide electrolyte. The main requirements for an oxide electrolyte material are that they remain stable at the operating temperature of the cell (typically greater than 500K) and that it is permeable to oxygen. The electrolyte should not undergo any phase transitions at the device's operating temperature. While zirconia is well suited for this application, pure zirconia can undergo phase transitions which limits its utility at the SOFC operating temperature. At 1 atm= 101325 Pa, cubic zirconia (space group Fm-3m) is stable at temperatures above 2500

K while the tetragonal phase (space group P42/nmc) is stable at 1450-2500 K, and the monoclinic (space group P21/c) is stable below 1400 K (Figure 1).

The cubic phase is stable only at high temperatures and pressures, and at lower temperatures, a mixture of two or more phases is present.[1] If varying phase compositions are present, the reliability of a device such as a SOFC would become compromised. It is desired that a single, stable phase be present for reliable device performance. It is well known that with the introduction of guest dopant atoms pure zirconia adopts a more thermally stable crystal phase.[2]

b) Stabilized Zirconia

Zirconia can be stabilized by the introduction of certain guest atoms, which allows it to be used more reliably in a variety of technologies. Doped stabilized zirconium has a wide variety of applications. They are used in automobile three-way catalysts, fuel cells, and dental implants.[3-6] Another application of YSZ is as a thermal barrier. YSZ has a low thermal conductivity which stays constant as temperature increases.[7] At values greater than 1500 K, the experimental thermal conductivity was still less than 5 W/mK.

The best-known and most commonly used of these is yttria-stabilized zirconia (YSZ) , in which Y^{3+} in are introduced as dopants stabilize the cubic phase compared to the monoclinic and tetragonal polymorphs.[3,8,9] It has been shown that the addition of only a small fraction of Y atoms to zirconia widens the temperature stability of the cubic phase.[10]

Since Y exists as a 3+ ion while Zr is a 4+ ion, the composition is actually $ZrY_xO_{(2+1.5x)}$ where x is the doping fraction, typically 0.08 or less. The addition of Y^{3+} to the system creates an oxygen deficiency compared to pure zirconia. This deficiency is believed to account for the increase in oxygen mobility.

YSZ is typically prepared by a combination of zirconium dioxide and yttrium dioxide.[11] This is commonly done by growing YSZ from a proportional mix of ZrO_2 and Y_2O_3. The yttrium stabilizes the cubic form of zirconia by a substitution of up to 8% of the Zr^{4+} with Y^{3+} ions.

c) Contemporary YSZ Preparative Methods.

There have been many published methods to synthesize YSZ, and one recently described method is prepared by forming alternating layers of zirconia (approximately 10 Å) and yttria (approximately 1 Å). This was done using both sputtering and atomic layer deposition (ALD).[11]

This method was used for a variety of reasons. For one, the researchers were able to produce a highly dense material with good electronic properties. This has paved the way for further ALD processing of the material so that high-aspect ratios (area to thickness) of YSZ for higher energy densities can be made.[11] Secondly, the researchers were able to exert a high level of conformity and tight control on the ALD-YSZ. This conformity and control extend to the stoichiometry, physical thickness, and interfacial properties of the ALD-YSZs.[11] Although the properties of the resulting YSZ are found to be within the desired range, little is known about the structural details of the material. Since YSZ is inherently non-crystalline, owing to the presence of guest atom defects, more traditional diffraction techniques to investigate the structural details are not especially informative. There have been some efforts to investigate YSZ using computational methods as outlined below[12-18], most of which were performed on bulk YSZ.

In this study, the goal is to investigate the structural properties of thin film deposited YSZ.

d) Investigation Rational

Further insight into the composition and structure of the prepared YSZ can be obtained using computational methods. Experimental methods are often difficult to interpret due to the inherent non-crystallinity of YSZ. Thus, molecular dynamics (MD) methods can provide an

understanding of the resulting materials. The following papers all include MD simulations to facilitate interpretation of experimental results.

Work was done by Brinkman et al., in which they investigated the oxygen diffusivity in $(ZrO_2)_{0.92}$ $(Y_2O_3)_{0.08}$.[12] In the creation of their model, they randomly replaced 16 Zr^{4+} with Y^{2+} and 8 O^{2-} with oxygen vacancies. By doing this, they started with YSZ and used that structure to analyze the diffusivity.

In a similar fashion, Lau and Dunlap investigated the oxygen ionic conductivity as a function of the mol% of YSZ.[13] This work is similar to the work done by Brinkman et al. in that both groups started with an initial YSZ structure. In Lau and Dunlap's work, a cubic fluorite lattice of ZrO_2 was generated and random Zr^{4+} ions were replaced with Y^{3+} ions. The oxygen vacancies were generated by randomly selecting anion sites and removing an O^{2-} ion resulting in a charge - neutral lattice. They then went on to make amorphous structures of YSZ. They found that for both crystal and amorphous YSZ, the peak ionic conductivity occurred at ~8.0 mol% Y_2O_3 consistent with experimental results.

Once again, this pattern is seen in the work of González-Romero et al. who were studying the grain boundaries in YSZ.[14] They studied the dependance of various properties at the grain boundaries in YSZ bicrystals and their dependence on temperature and concentration of yttria. To make the YSZ structure, they randomly replaced Zr^{4+} with Y^{3+} and they introduced enough oxygen vacancies to keep the system at a neutral charge.

Schelling and Phillpot did research on various aspects of YSZ.[15,16] In one paper, they investigated the thermal conductivity, κ, of both pure ZrO_2 and YSZ.[15] They found that the high-temperature κ of pure ZrO_2 and YSZ with low concentrations of Y_2O_3 was similar to that of a crystalline solid, and that the dominant factor was photon-photon scattering. However, at higher

concentrations of Y_2O_3, the mechanism becomes more typical of an amorphous system. Specifically, only at very low frequencies do photonlike vibrational modes exhibiting well-defined wave vectors appear. In another paper, Schelling, Phillpot, and Wolf investigated the phase transition from cubic to tetragonal in YSZ and ZrO_2.[16] They concluded that the transition is first-order as there is a discontinuous change in volume and in the latent heat of transition. In addition, they also showed that the transition is displacive. Their model was also to predict that the doping with yttria tends to stabilize the cubic phase at lower temperatures. In the first paper, the YSZ was prepared with Zr^{4+} ions randomly substituted with Y^{3+} ions and for every two yttrium ions added, one oxygen ion was removed to keep the charge neutral. In the latter paper, they started with a cubic structure and randomly distributed vacancies and yttrium ions. For every two yttrium ions added, a vacancy needed to be introduced. It is assumed they did a similar formation of YSZ for both papers.

Arima et al. investigated various properties of YSZ including lattice structure and the dynamic and thermal properties.[17] They found that the lattice constant increased with temperature and yttria content. They also found that the self-diffusion of O^{2-} was greater than that of Zr^{4+} and Y^{3+} and that it decreased as the yttria content increased. At 1500 K, the oxygen self-diffusion constant determined by the MD simulations was reported as 1.2×10^{-10} m^2/s. The heat capacity at constant pressure was in good agreement with experimental data when the anharmonic term was estimated using experimental thermal expansion coefficients and elastic constants but the anharmonic term from MD simulation was not reliable for the thermal over the wide range of temperature. This shows that there is a limitation of rigid-ion approximation for interatomic potential used in current MD simulations. Similar to previous papers, they formed the YSZ structure by having Y^{3+} and oxygen vacancies randomly replace Zr^{4+} and O regular sites.

Yamamura et al. studied the ionic conductivity of YSZ at varying Y_2O_3 concentrations.[18] Similar to experimental results, they found that the thermal conductivity maximum occurred at 8 mol% Y_2O_3. They continued this research by determining the positions of the oxygen vacancies and determined that the oxygen vacancies are trapped at the second neighbor position to Y^{3+} ions. They also found that the number of sites that trap the vacancies increased with Y_2O_3 concentration, causing a trade-off between the increase in the number of vacancies and a decrease of the mobility of the vacancies. This is considered to be the reason that the maximum ionic conductivity occurs at 8 mol% Y_2O_3. Unlike other research previously discussed, Yamamura et al. used two distributions of yttrium ions. In one, they randomly arranged the ions in cation sites, and in the second they manually arranged the ions so as to not occupy the nearest neighbor position to each other.

Despite all the interesting MD simulations done in the past, most/all of these were performed on small systems using implanted Y dopant ions in an otherwise bulk crystal. In the work of Molina-Reyes and in many other experimental synthetic strategies, thin films of Y_2O_3 are deposited onto a zirconia surface and annealed to yield the resulting YSZ[11]. In such preparations, it is difficult to establish the concentration gradient that would likely result, as well as the structural aspects of the YSZ. For example, does such a preparative method lead to a greater likelihood of Y ion clustering near the surface; how does the oxygen mobility vary with surface depth; and what is the rate of the Y diffusion into the zirconium bulk layer? In this study, we investigate large scale (10s of thousands of atoms) systems composed of bulk zirconium and yttria films. The goal of these studies is to determine some of the properties of the YSZ prepared using surface film annealing as well as the parameters that yield reliable MD simulations.

Methodology

Unless otherwise stated, all figures were created by the author and his research group.

The molecular dynamics (MD) simulation requires an initial structure and a set of interaction potentials that estimate the interatomic interaction between atom pairs. The process for the simulation follows a scheme in which the initial atomic configuration is prepared. In the first step, the coordinates of each atom are changed to a new location according to the integrated Newton's equations of motion.

$$r(t + dt) = r(t) + v \cdot dt + \frac{a \cdot dt^2}{2} \quad (1)$$

Where r is the atomic coordinate, v is the atomic velocity, and a is the atomic acceleration. The initial velocity for each atom is determined by the program using a random number generator. The updated velocity is obtained using Equation 2.

$$v(t + dt) = v(t) + a \cdot dt \quad (2)$$

The acceleration term is determined using the force field potential.

$$F = m \cdot a$$

$$a = \frac{F}{m} \quad (3)$$

The force on each atom is calculated through a series of potentials that include electrostatic and soft van der Waals interactions.

The electrostatic potential takes the form of Coulomb's Law:

$$V_{ij} = \frac{q_i q_j}{4\pi\varepsilon_0 r_{ij}} \quad (4)$$

In Equation 4, q is the charge of the ions (-2 for oxygen, +3 for yttrium, and +4 for zirconium), ε_0 is the permittivity of the vacuum, and r_{ij} is the distance between the ions. For two-unit charge ions separated by 5 Å, the potential is 2.9 eV. Van der Waals (non-ionic) interactions are handled by a fitted potential in classical MD, and many such potentials have been developed in the past. One of the most commonly used potentials for metal oxides is the Buckingham potential, which was first introduced in 1938:[19]

$$V_{Buck} = Ae^{-\frac{r_{ij}}{\rho}} - \frac{C}{{r_{ij}}^6} \quad 5^{19}$$

In Equation 5, A, ρ, and C are fitted parameters specific to a particular atom pair. The first term is positive and provides the repulsive interactions, while the second term is negative and provides the attractive interactions. Several parameter sets from recent literature for YSZ are provided in Table 1: It is common for the metal-oxides potentials to neglect the attractive term (C=0). This provides greater stability in the potential. In addition, since it is unlikely for metal-metal interactions to be present at closer interactions, only the O-O and O-metal potentials are presented. Ignoring the metal-metal interactions also allows for greater computational efficiency since less atom pairs are being calculated. Figure 2 shows a plot for the Schelling potential set. Only the O-O interaction set includes a non-zero attractive term while both the Zr-O and Y-O potentials only include a repulsive term. This is commonly done in metal oxide MD simulations for two reasons. First, reliable results are achieved in the absence of a repulsive term. Second, the simulation has greater computational efficiency with fewer potential terms. Also, the Zr-O and Y-O terms have very similar A and ρ values and so the plots for these in Figure 2 are essentially overlapping.

Table 1. Buckingham interatomic potentials for oxygen, zirconium, and yttrium interactions

Ion pair	A (eV)	ρ(Å)	C (eV·Å^6)
	Schelling[16]		
O-Zr	1502.09	0.345	0.0
O-O	9547.88	0.224	19.60
Y-O	1366.32	0.348	0.0
	Brinkman[12]		
O-Zr	985.85	0.376	0.0
O-O	22759.44	0.149	27.89
Y-O	1345.0	0.349	0.0
	Lau[13]		
O-Zr	1292.85	0.353	19.36
O-O (Zr)	13098.9	0.2196	49.30
O-Y	1642.7	0.3532	104.18
O-O (Y)	2056.5	0.3614	271.76

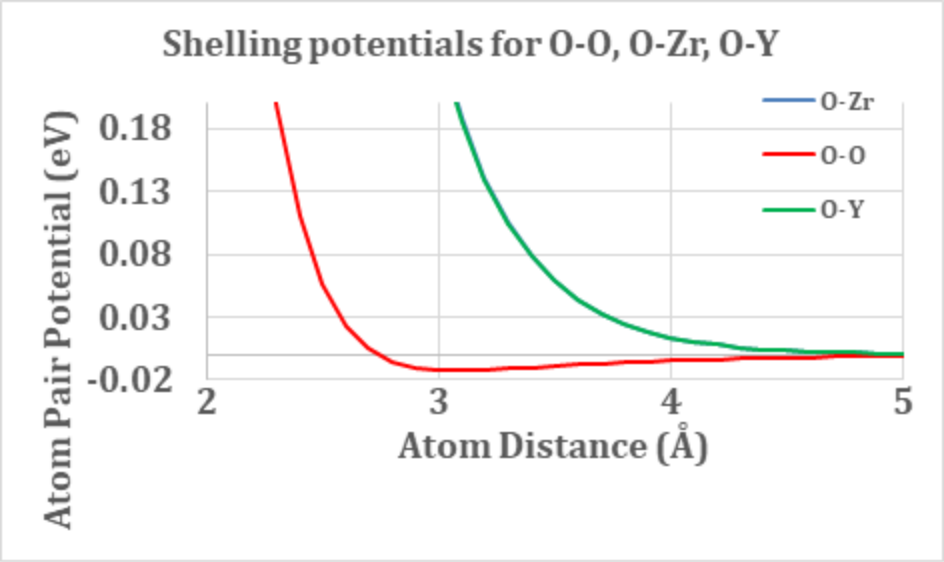

Figure 2. Interatomic pair potentials for the Schelling set.

For the simulations in this research, the potentials from Schelling et al. were selected. This is because of the prior research performed by other members of the Center for Computational Research, Jacob Gartlgruber, Maximilian Krejpowicz, Tom Melfi, Anastasis Rubino, and Stephen Kelty using The General Utility Lattice Program (GULP).[20] From that study, it was determined that the Schelling potential set performed the best out of the three potentials listed in Table 1, although the differences were minimal. This determination was made by calculating an approximate Figure of Merit (FOM) for each potential set (Equation 6).

$$FOM = \sqrt{(\%\Delta V)^2 + (\%\Delta F)^2} \qquad 6$$

Where ΔV and ΔF are the changes in the cell volume and fractional coordinates in the optimized ZrO_2 or Y_2O_3 call using each potential set. From this study, it was concluded that the minimal FOM, which corresponds to the optimal potential set, was found to be the Schelling potentials (see Tables 2 and 3).

Table 2. Figure of Merit for ZrO_2.

Space Group	Lattice type	S.G #	F.O.M.		
			ZrO_2		
			Schelling	Brinkman	Lau/Dunlop
$Fm\bar{3}m$	Cubic	225	**1.75**	4.3	4.6
$P4_2/nmc$	Tetragonal	137	**1.34**	2.2	2.5
$Pnma$	Orthorhombic	62	**22.9**	24.2	24.2
$Pbca$	Orthorhombic	61	**11.0**	21.5	13.0
$P2_1/c$	Monoclinic	14	**29.7**	29.4	29.4

Table 3. Figure of Merit for Y_2O_3.

Space Group	Lattice type	S.G #	F.O.M.		
			Y_2O_3		
			Schelling	Brinkman	Lau/Dunlop
$Ia\bar{3}$	Cubic	206	**6.3**	5.7	11.3
$R\bar{3}c$	Trigonal	167	**5.0**	6.2	12.0
$P\bar{4}m2$	Tetragonal	115	**1.9**	4.5	9.3
$P2_1/m$	Monoclinic	11	**3.6**	5.3	10.4

The MD simulations are performed by selecting a short-range interaction potential along with the electrostatic potential to form the basis for inter-atomic interactions. Using the equations of motion (Equations 1-3) and the derivative of the potentials in Equations 4 and 5, all the terms needed to perform a time trajectory are available. The time interval for each step (time-step) is selected so as to provide sufficient sampling for expected atomic motion. The fastest motion is vibration which typically has a period of 10^{-12} to 10^{-13} seconds. In most cases, a time-step of 1 fs is found to be sufficient, which is what was used in this study. Over a preselected time interval (time-step), which is on the order of magnitude of a few femtoseconds, the force on each particle is calculated from the interaction potentials to find the acceleration. Over the timestep, the particles are moved to a new position and a new force and acceleration are calculated. This process is repeated over the trajectory. The simulations are executed under constraints such as constant

temperature (T), volume(V), pressure (P), number of particles (N), or energy (E). In this study, the calculations were carried out under constant NVT (canonical ensemble) conditions. The temperature is controlled using the average velocity using the classical relation:

$$T = \frac{m\langle\vec{v}\rangle^2}{3k_B} \quad (7)$$

In Equation 7, k_B is the Boltzman constant, T is the desired temperature, m is the particle mass, and $\langle\vec{v}\rangle$ is the average velocity. By scaling the velocity up or down, the temperature can be controlled. The algorithm used in these studies was one introduced by Barendson.[21] The algorithm scales the velocity needed to maintain the desired temperature by using a damping factor that prevents wild temperature swings. No specific control is needed to maintain constant N or V.

Once the interaction potentials end constraint ensembles are selected, the initial structure is created.

The zirconia layer was created by cleaving cubic zirconia (Fm-3m) along the (110) plane (Figure 3). This surface was selected since there would be no dipole normal to the plane which often results in artificial instability at the surface. This surface unit cell was expanded to create the initial slab of the zirconia (Figure 4).

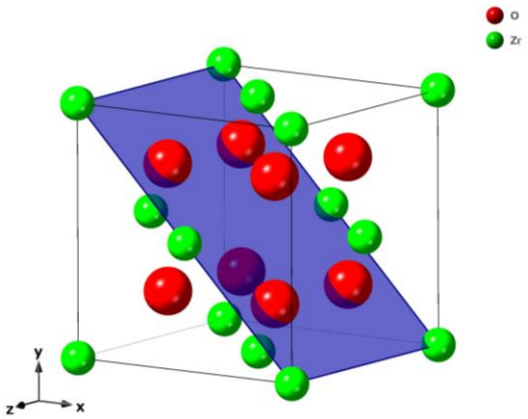

Figure 3. (110) plane of cubic zirconia used for simulations.

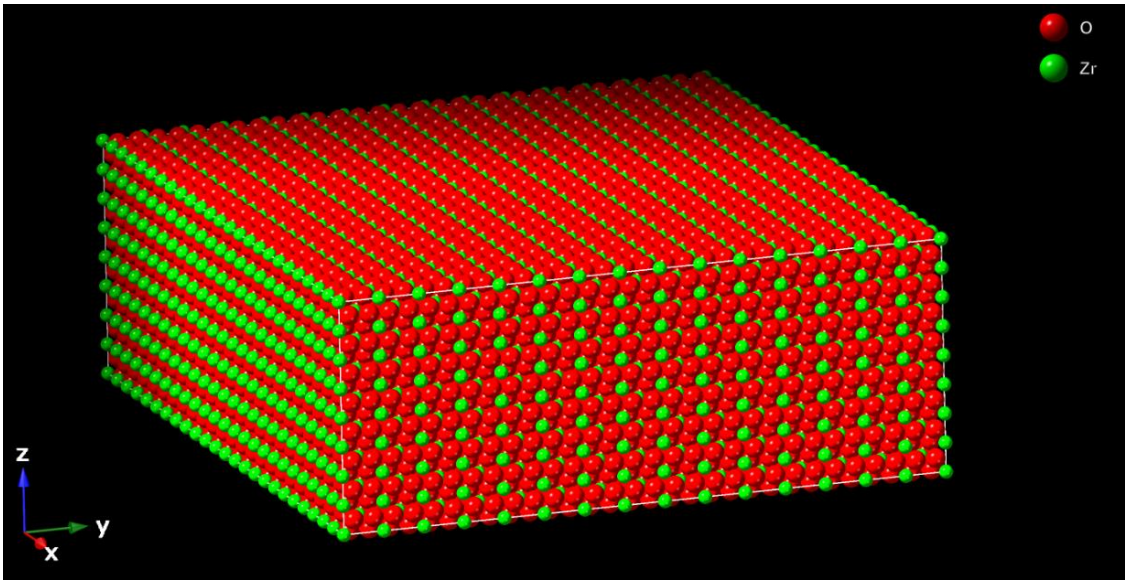

Figure 4. Expanded zirconia slab.

Above the zirconia slab, a 30 Å vacuum layer was added. This allows for the surface zirconia to undergo amorphization. The bottom 3-4 atomic layers were held fixed to approximate bulk zirconia. The zirconia slab was first run at increasing temperatures to cause amorphization of the surface in order to more closely approximate the surface where the subsequent yttria layer is deposited. In all simulations, periodic boundary conditions were used.

The trials were done using Large-scale Atomic/Molecular Massively Parallel Simulator (LAMMPS).[22] In initial trials, an attempt was made to replicate the exact structure used in the paper by Molina-Reyes et al. by having one layer of zirconia followed by one layer of yttria with no vacuum or fixed layer atoms. This model contained alternating layers of 10 Å of (110) ZrO_2 and 1 Å of (110) oriented cubic (Ia-3) Y_2O_3 that Molina-Reyes et al. worked with. However, this system showed no diffusion of yttrium into the zirconia layers even after extended simulation times at elevated constant temperature. Since the structure did not contain any vacuum layer that would allow for lattice expansion that would allow for defect diffusion, it is concluded that these

structures may not be suitable for modeling using methods employed or may take exceedingly long simulation times. Further tests were done with samples that contained a vacuum above the slab.

After the trials with alternating zirconia and yttria, a slab system was created contingent the base slab of (110) Fm-3m ZrO_2 as shown in Figure 7 on which a slab of (110) Ia-3 was subsequently added (Figures 5 and 6) in order to achieve a ZrO_2 surface that closely approximated an as-grown surface, the ZrO_2 slab was first equilibrated before adding the Y_2O_3 layer.

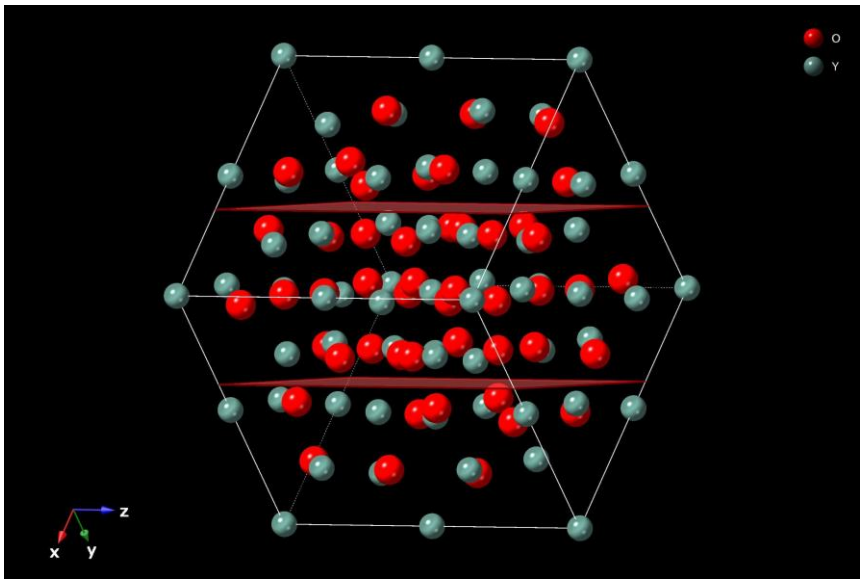

Figure 5. Cleaving of the yttria using two planes (orange).

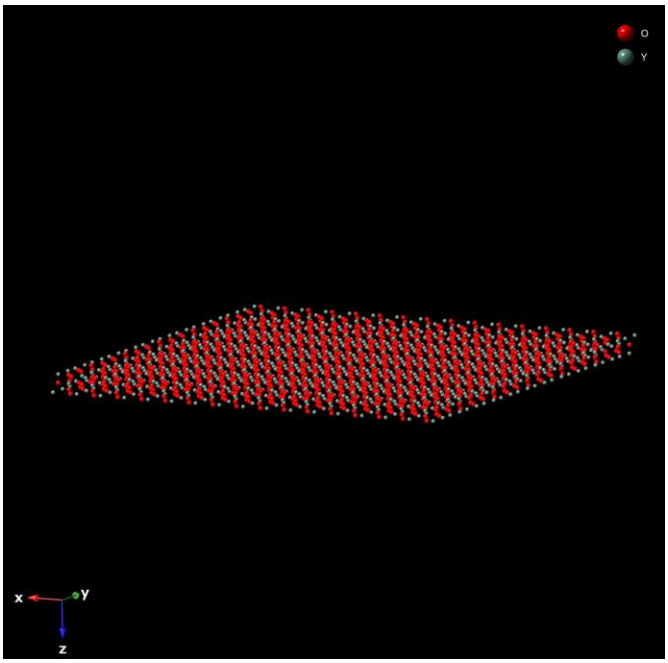

Figure 6. 6x8 yttria slab.

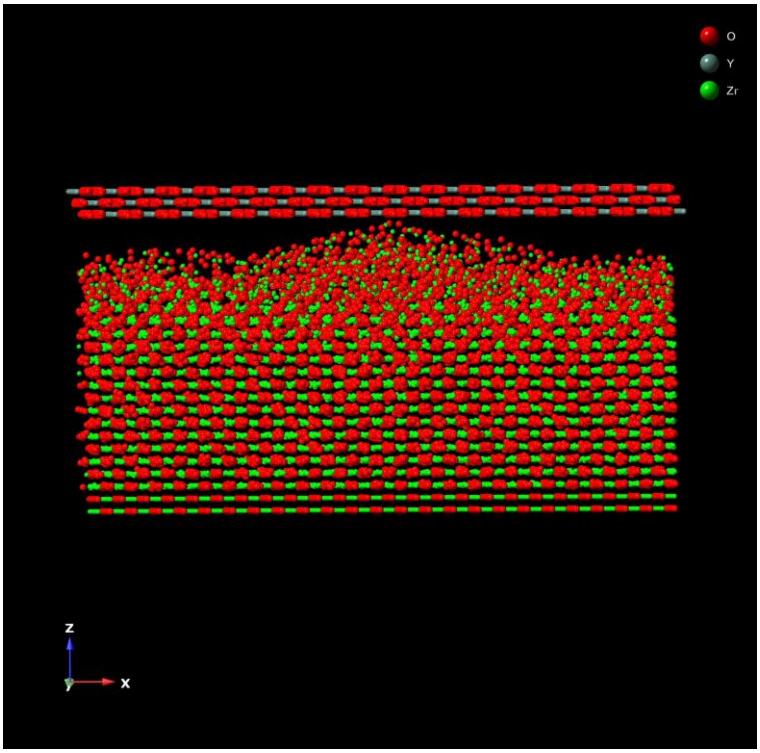

Figure 7. Expanded yttria slab placed on zirconia slab.

For the ZrO_2, a slab/vacuum system of 87.40 Å x 77.23 Å lateral dimension and 29.13 Å thickness was run at increasing temperatures (as shown in Table 4).

Table 4. Length and temperatures for the zirconia layer trials.

Run	Timesteps (fs)	Temperature (K)	Fixed atoms length (Å)
1	10,000	300	0 - 21
2	10,000	300	0 - 4
3	100,000	600	0 - 4
4	100,000	900	0 - 4
5	200,000	1200	0 - 4
6	500,000	1500	0 - 4

The resulting equilibrated base ZrO_2 slab is shown in Figure 7. The surface shows a degree of roughness and amorphization typical of as-grown surfaces.

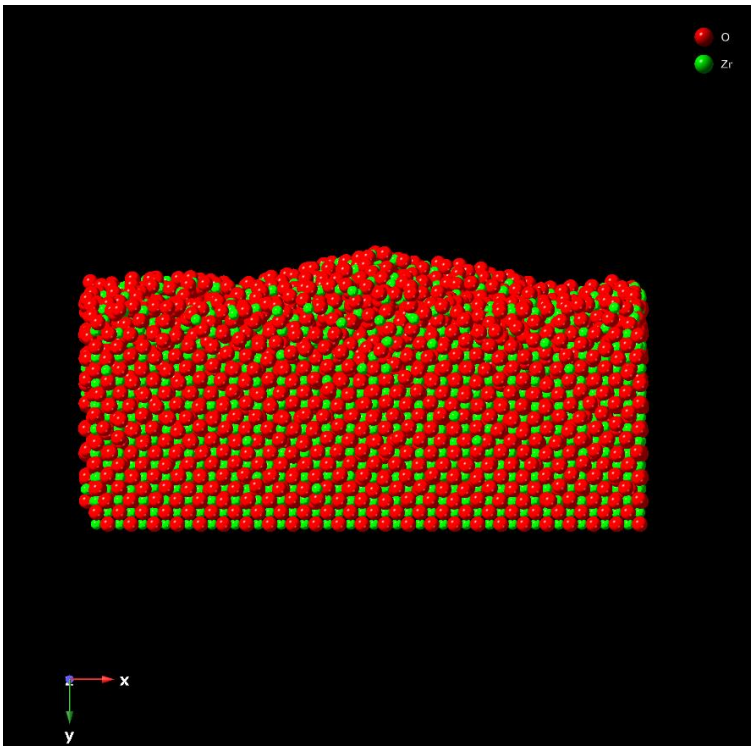

Figure 8. ZrO_2 base layer following equilibration.

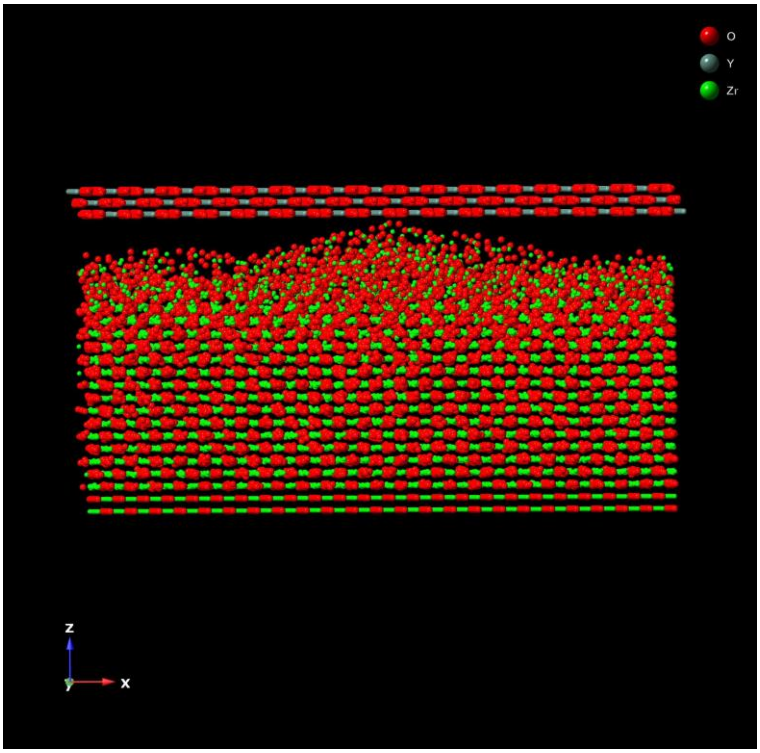

Figure 9. Expanded yttria slab places on zirconia slab.

Following the base slab equilibration, a 10.1 Å layer of Ia-3 (110) yttria was placed above the equilibrated ZrO_2 slab as shown in Figure 11. This system had approximately 30 Å of vacuum above it. Similar to the previous trials, the system was heated at various temperatures for various lengths (See Table 5). The difference between the first two trials is the number of frozen atoms. In run 1, the entire zirconia layer was fixed, whereas in all subsequent runs, only the bottom 4 Å of the ZrO_2 slab was fixed.

Table 5. Length and temperatures for trials with both layers.

Run Number	Timesteps (fs)	Temperature (K)
1	10,000	300
2	10,000	300
3	10,000	600
4	100,000	900
5	200,000	1200
6	500,000	1500
7	1,250,000	1500
8	1,250,000	1500
9	1,250,000	1500
10	1,250,000	1500

The resulting system following run 10 is shown in Figure 9. The yttria layer has adsorbed onto the zirconia slab and begun to diffuse into it.

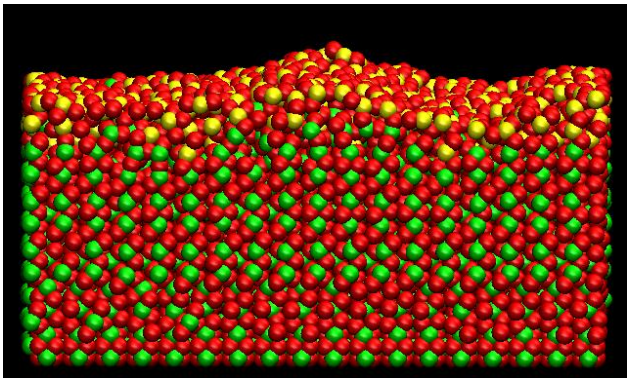

Figure 10. Final state of the Y_2O_3/ZrO_2 system.

Results

The last time-step in run 10 is analyzed to ensure the temperature and total energy were consistent for the entirety of the run (Figures 10 and 11). These figures include a linear least square fit which indicates that the slope is minimal. This shows that the system is equilibrated. While there was some variation in the temperature, the value always deviated by less than 3% of the desired temperature.

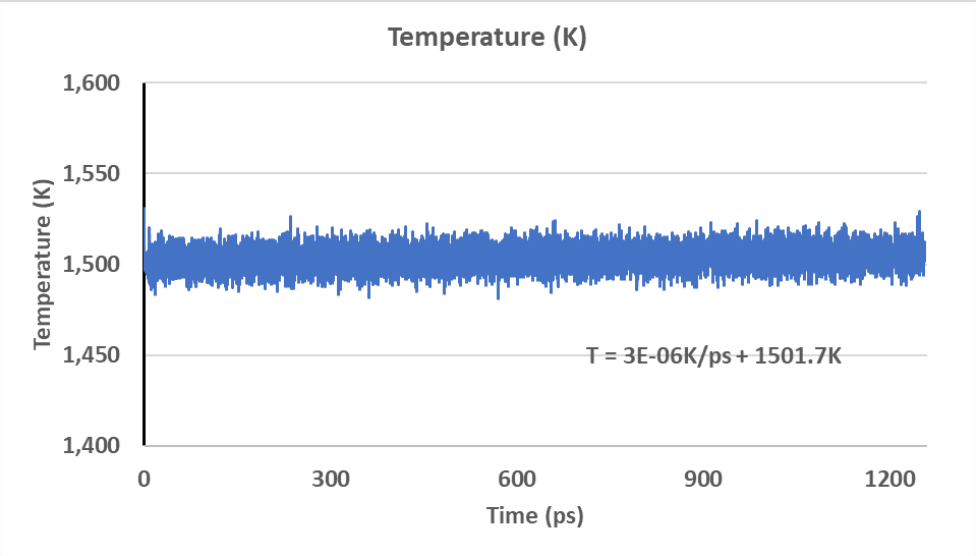

Figure 11. Temperature trace for run 10.

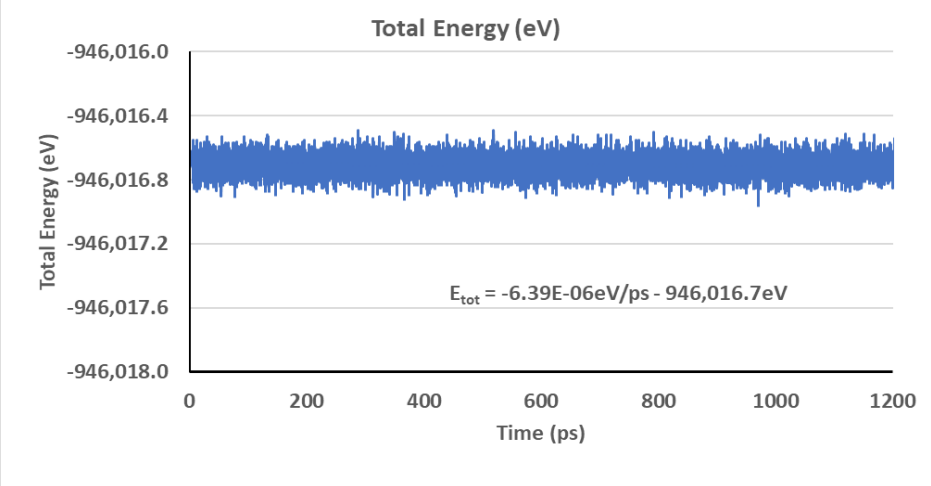

Figure 12. Total energy trace for run 10.

A depth profile of the final run showing atomic composition is shown in Figure 13.

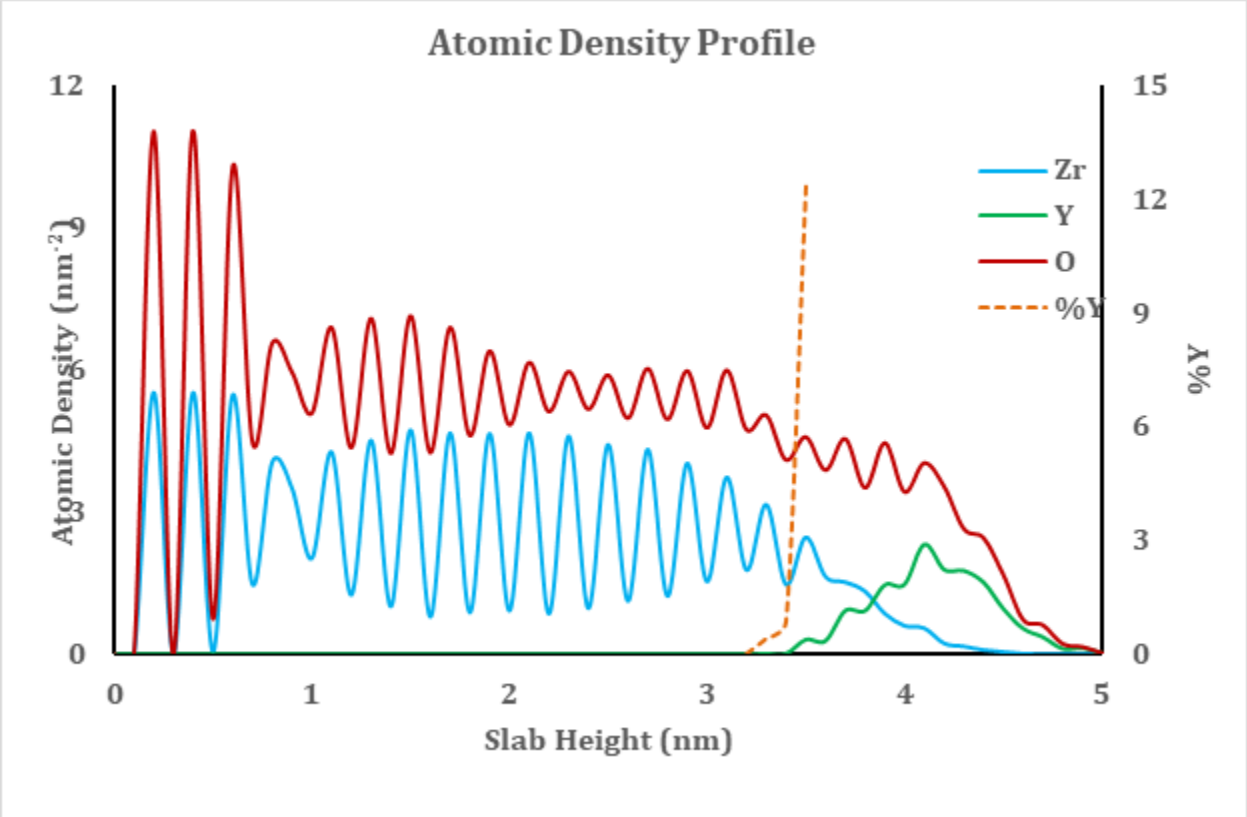

Figure 13. Depth profile composition of the final run.

Figure 14 shows that in the first several atomic layers (0-0.05 nm) were held fixed throughout the simulations and the selected (110) orientation contains a 1:2 Zr:O ratio. Above the fixed layers, the crystal indicates that an alternate crystalline orientation was adopted persisting up to approximately 30 Å. These layers show a regular repeating crystal phase which is an important indication that the crystal has not melted into an amorphous phase. If it had done so, further analysis would not be representative of crystalline YSZ. This more stable orientation (at 1500 K) is of an at present undetermined phase, and, while not part of the focus of this study, may yield interesting properties of the ZrO_2 phase. Further investigation of that aspect of the results may be warranted. The topmost layers, near the yttria layer slab, indicate diffusion of Y atoms into the ZrO_2. Likewise, it appears that Zr atoms have diffused into the yttria layer. Also shown in Figure

14 is the plot of the % fraction of Y compared to Zr. The typical range of % in functional YSZ material is less than 12% and so the range of 30-35 Å is analyzed in the following section.

The root mean square displacement (RMSD) of the atoms from their initial coordinates is described by:

$$RMSD = \sqrt{\langle (r_0 - r_t)^2 \rangle} \quad 8$$

In Equation 5, r_0 is the initial coordinate and r_t is the coordinate at time t. The RMSD is the square root of the average of the square of the displacements. From the RMSD, the diffusion coefficient D can be obtained from the Einstein-Smoluchowski equation:

$$D = \frac{(RMSD)^2}{6t} \quad 9$$

The last time-was also analyzed using Visual Molecular Dynamics (VMD)[23] to obtain a plot of the RMSD for oxygen in the range z=30-35 Å (where the Y% is ca. 1-10%, see Figure 14) is shown in Figure 15.

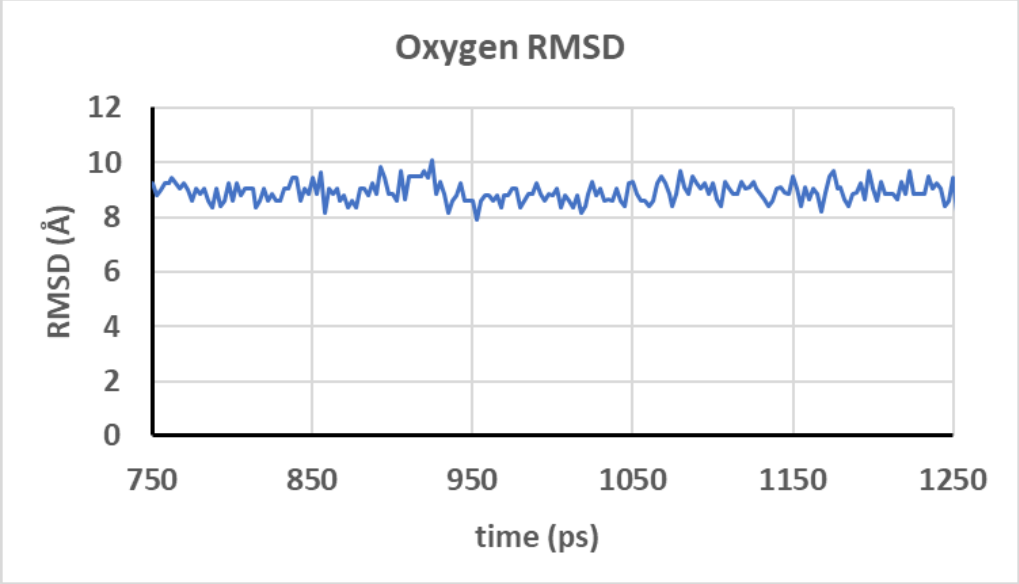

Figure 14. RMSD for oxygen in final equilibrium trajectory.

The last For the RMSD plot, the first 500 ps were excluded from the analysis because the system was not stable. The final 725 ps were used for analysis. For oxygen in this range, the

calculated diffusion coefficient (Equation 6) was found to be $D=1.35\times10^{-10}$ m^2/s. This value compares favorably with previously reported results for both MD simulations and experimental results[17,24]. The present results are slightly greater than previously reported (ca 1.2×10^{-10} m^2/s) for 1500 K. Some considerations are in order. First, diffusion in a bulk crystal would normally be expected to be less than in a surface. Bulk systems require displacement of neighboring atoms which are expected to have significantly greater barriers than in a surface region. Second, for the range in which the diffusion was calculated, the Y% varies from <1% to over 10% which would cause some variability. The prior work, however, did not show a significant variation in D over the range greater than 10% Y doping and, in fact, showed decreasing diffusion as a function of increasing Y%. As a comparison to a region with no influence of Y atoms (z=10-15 Å), see Figure 14), the oxygen diffusion coefficient is found to be $< 1\times10^{-10}$ m^2/s.

Conclusion

In this study, an analysis of the formation of YSZ starting from thin films of Y_2O_3 on a ZrO_2 slab was carried out using MD simulations. An initial attempt was made to replicate the work of Molina-Reyes et al. with alternating Y_2O_3 and ZrO_2; however, this proved to be unsuccessful as the zirconia layer did not appear to allow sufficient defect formation for yttria to diffuse into it in a reasonable time frame at the ensemble temperature used. Higher temperatures might have allowed this to happen but would likely result in melting the crystal which would render it unsuitable for comparison with experimental synthetic methods.

A more successful approach was found by making a slab of zirconia and first amorphizing the surface to allow for defects in the crystal structure. In fact, this likely approximated an as-grown zirconia film more closely. A slab of yttria was then placed on top of the amorphized slab with vacuum above it. This allowed for the yttria to diffuse into the zirconia and a diffusion coefficient (D) for oxygen was found. D was found to be 1.35×10^{-10} m^2/s and was in good agreement with previous literature.

It is noted that in the region first fixed by zirconia and the interfacial region, the zirconia appeared to undergo a phase transition to either an alternate cubic orientation or an alternate crystal phase than cubic. While not a specific goal of this project, further investigation of the identity of that phase might be of interest.

References

1. Bouvier, P.; Djurado, E.; Lucazeau, G.; Bihan, T. High-Pressure Structural Evolution of Undoped Tetragonal Nanocrystalline Zirconia. *Phys. Rev. B* **2000**, *62*, 8731–8737. https://doi.org/10.1103/PhysRevB.62.8731.
2. Adler, S. B. Factors Governing Oxygen Reduction in Solid Oxide Fuel Cell Cathodes. *Chem. Rev.* **2004**, *104* (10), 4791–4844. https://doi.org/10.1021/cr020724o.
3. Meredig, B.; Wolverton, C. Dissolving the Periodic Table in Cubic Zirconia: Data Mining to Discover Chemical Trends. *Chem. Mater.* **2014**, *26* (6), 1985–1991. https://doi.org/10.1021/cm403727z.
4. Colón, G.; Pijolat, M.; Valdivieso, F.; Vidal, H.; Kašpar, J.; Finocchio, E.; Daturi, M.; Binet, C.; C. Lavalley, J.; T. Baker, R.; Bernal, S. Surface and Structural Characterization of CeZr1-O2 CEZIRENCAT Mixed Oxides as Potential Three-Way Catalyst Promoters. *J Chem Soc Faraday Trans* **1998**, *94* (24), 3717–3726. https://doi.org/10.1039/A807680D.
5. Singhal, S. Advances in Solid Oxide Fuel Cell Technology. *Solid State Ion.* **2000**, *135* (1–4), 305–313. https://doi.org/10.1016/S0167-2738(00)00452-5.
6. Denry, I.; Kelly, J. State of the Art of Zirconia for Dental Applications. *Dent. Mater.* **2008**, *24* (3), 299–307. https://doi.org/10.1016/j.dental.2007.05.007.
7. Clarke, D. R.; Phillpot, S. R. Thermal Barrier Coating Materials. *Mater. Today* **2005**, *8* (6), 22–29. https://doi.org/10.1016/S1369-7021(05)70934-2.
8. De Souza, S. Thin-Film Solid Oxide Fuel Cell with High Performance at Low-Temperature. *Solid State Ion.* **1997**, *98* (1–2), 57–61. https://doi.org/10.1016/S0167-2738(96)00525-5.

9. Fabris, S.; Paxton, A.; Finnis, M. A Stabilization Mechanism of Zirconia Based on Oxygen Vacancies Only. *Acta Mater. V50 5171-5178 2002* **2002**, *50*. https://doi.org/10.1016/S1359-6454(02)00385-3.

10. Liu, T.; Zhang, X.; Wang, X.; Yu, J.; Li, L. A Review of Zirconia-Based Solid Electrolytes. *Ionics* **2016**, *22*. https://doi.org/10.1007/s11581-016-1880-1.

11. Molina-Reyes, J.; Tiznado, H.; Soto, G.; Vargas-Bautista, M.; Dominguez, D.; Murillo, E.; Sweeney, D.; Read, J. Physical and Electrical Characterization of Yttrium-Stabilized Zirconia (YSZ) Thin Films Deposited by Sputtering and Atomic-Layer Deposition. *J. Mater. Sci. Mater. Electron.* **2018**, *29* (18), 15349–15357. https://doi.org/10.1007/s10854-018-8909-3.

12. Brinkman, H. W.; Briels, W. J.; Verweij, H. Molecular Dynamics Simulations of Yttria-Stabilized Zirconia. *Chem. Phys. Lett.* **1995**, *247* (4), 386–390. https://doi.org/10.1016/S0009-2614(95)01231-1.

13. Lau, K. C.; Dunlap, B. I. Molecular Dynamics Simulation of Yttria-Stabilized Zirconia (YSZ) Crystalline and Amorphous Solids. *J. Phys. Condens. Matter* **2011**, *23* (3), 035401. https://doi.org/10.1088/0953-8984/23/3/035401.

14. Gonzalez-Romero, R. L.; Melendez, J. J.; Gomez-Garcia, D.; Cumbrera, F. L.; Dominguez-Rodriguez, Arturo. A Molecular Dynamics Study of Grain Boundaries in YSZ: Structure, Energetics and Diffusion of Oxygen. *Solid State Ion.* **2012**, *219* (Copyright (C) 2018 American Chemical Society (ACS). All Rights Reserved.), 1–10. https://doi.org/10.1016/j.ssi.2012.05.004.

15. Schelling, P. K.; Phillpot, S. R. Mechanism of Thermal Transport in Zirconia and Yttria-Stabilized Zirconia by Molecular-Dynamics Simulation. *J. Am. Ceram. Soc.* **2001**, *84* (Copyright (C) 2018 American Chemical Society (ACS). All Rights Reserved.), 2997–3007. https://doi.org/10.1111/j.1151-2916.2001.tb01127.x.

16. Schelling, P. K.; Phillpot, S. R.; Wolf, D. Mechanism of the Cubic-to-Tetragonal Phase Transition in Zirconia and Yttria-Stabilized Zirconia by Molecular-Dynamics Simulation. *J. Am. Ceram. Soc.* **2001**, *84* (7), 1609–1619. https://doi.org/10.1111/j.1151-2916.2001.tb00885.x.

17. Arima, T.; Fukuyo, K.; Idemitsu, K.; Inagaki, Y. Molecular Dynamics Simulation of Yttria-Stabilized Zirconia between 300 and 2000 K. *J. Mol. Liq.* **2004**, *113* (Copyright (C) 2018 American Chemical Society (ACS). All Rights Reserved.), 67–73. https://doi.org/10.1016/j.molliq.2004.02.038.

18 Yamamura, Y.; Kawasaki, S.; Sakai, Hiroaki. Molecular Dynamics Analysis of Ionic Conduction Mechanism in Yttria-Stabilized Zirconia. *Solid State Ion.* **1999**, *126* (Copyright (C) 2018 American Chemical Society (ACS). All Rights Reserved.), 181–189. https://doi.org/10.1016/S0167-2738(99)00227-1.

19. Buckingham, R. A. The Classical Equation of State of Gaseous Helium, Neon and Argon. *Proc. R. Soc. Lond. Ser. Math. Phys. Sci.* **1938**, *168* (933), 264–283. https://doi.org/10.1098/rspa.1938.0173.

20. Gale, J. D.; Rohl, A. L. The General Utility Lattice Program (GULP). *Mol. Simul.* **2003**, *29* (5), 291–341. https://doi.org/10.1080/0892702031000104887.

21. Berendsen, H. J. C.; Postma, J. P. M.; Van Gunsteren, W. F.; DiNola, A.; Haak, J. R. Molecular Dynamics with Coupling to an External Bath. *J. Chem. Phys.* **1984**, *81* (8), 3684–3690. https://doi.org/10.1063/1.448118.

22. Thompson, A. P.; Aktulga, H. M.; Berger, R.; Bolintineanu, D. S.; Brown, W. M.; Crozier, P. S.; in 't Veld, P. J.; Kohlmeyer, A.; Moore, S. G.; Nguyen, T. D.; Shan, R.; Stevens, M. J.; Tranchida, J.; Trott, C.; Plimpton, S. J. LAMMPS - a Flexible Simulation Tool for Particle-

Based Materials Modeling at the Atomic, Meso, and Continuum Scales. *Comput. Phys. Commun.* **2022**, *271*, 108171. https://doi.org/10.1016/j.cpc.2021.108171.

23. Humphrey, W.; Dalke, A.; Schulten, K. VMD: Visual Molecular Dynamics. J. Mol. Graph. 1996, 14 (1), 33–38. https://doi.org/10.1016/0263-7855(96)00018-5.

24. Oishi, Y.; Ando, K. Oxygen Self-Diffusion in Cubic ZrO2 Solid Solutions. In *Transport in Nonstoichiometric Compounds*; Simkovich, G., Stubican, V. S., Eds.; NATO ASI Series; Springer US: Boston, MA, 1985; pp 189–202. https://doi.org/10.1007/978-1-4613-2519-2_15.